Chaos in Schwarzschild spacetime: The motion of a spinning particle

Shingo Suzuki* and Kei-ichi Maeda†
Department of Physics, Waseda University, Shinjuku-ku, Tokyo 169, Japan
(Received 9 April 1996)

We study the motion of a spinning test particle in Schwarzschild spacetime, analyzing the Poincaré map and the Lyapunov exponent. We find chaotic behavior for a particle with spin higher than some critical value (e.g., $S_{\rm cr}\sim 0.635\mu M$ for the total angular momentum $J=4\mu M$), where μ and M are the masses of a particle and of a black hole, respectively. The inverse of the Lyapunov exponent in the most chaotic case is about five orbital periods, which suggests that chaos of a spinning particle may become important in some relativistic astrophysical phenomena. The ''effective potential'' analysis enables us to classify the particle orbits into four types as follows. When the total angular momentum J is large, some orbits are bounded and the ''effective potentials'' are classified into two types: (B1) one saddle point (unstable circular orbit) and one minimal point (stable circular orbit) on the equatorial plane exist for small spin; and (B2) two saddle points bifurcate from the equatorial plane and one minimal point remains on the equatorial plane for large spin. When J is small, no bound orbits exist and the potentials are classified into another two types: (U1) no extremal point is found for small spin; and (U2) one saddle point appears on the equatorial plane, which is unstable in the direction perpendicular to the equatorial plane, for large spin. The types (B1) and (U1) are the same as those for a spinless particle, but the potentials (B2) and (U2) are new types caused by spin-orbit coupling. The chaotic behavior is found only in the type (B2) potential. The ''heteroclinic orbit,'' which could cause chaos, is also observed in type (B2). [S0556-2821(97)06806-9]

PACS number(s): 04.70.Bw, 95.10.Fh

I. INTRODUCTION

Chaos is now one of the most important ideas used to explain various nonlinear phenomena in nature. Since the research on the three-body problem by Poincaré, many studies about chaos in celestial mechanics and astrophysics have been done and have revealed the important role of chaos in the Universe [1,2]. Although we know many features of chaos in Newtonian dynamics, we do not know, so far, so much about those in general relativity. If gravity is strong, e.g., a close binary system or a particle near a black hole, we have to use Einstein's theory of gravitation. Because the gravitational field in general relativity is nonlinear, we may find a new type of chaotic behavior in strong gravitational fields, which does not appear in Newtonian dynamics [3–5]. In a previous paper [6], we studied a criterion for chaos of a test particle motion around an N-black hole system (or an N-naked singularity system) and found that a local instability determined by the Riemann curvature tensor provides us a sufficient test for chaos. We also found that the existence of an unstable circular orbit, which guarantees the existence of a homoclinic or heteroclinic orbit, plays a crucial role for chaos. However, the relativistic systems analyzed so far by several authors [6–13], in which chaotic behavior of a test particle is found, are rather unrealistic [6–11], except for the perturbed spacetimes of the Schwarzschild black hole solution [12,13]. As for the other interesting cases of systems, for example, the N-extreme black hole system [7–9] is unstable, the existence of a strong uniform magnetic field around a black hole [10] is not likely, and naked singularities [6] may not exist. We may wonder whether any realistic relativistic system can be chaotic and when chaos may play an important role in such a relativistic astrophysical phenomena.

In astrophysics, rotation of a system plays a quite important role. The angular momentum or spin may completely change the evolution of the system. In a dynamical system, rotation or spin is one of the most important elements and it may sometime cause chaotic behavior. We also know that some spin-orbit interaction induces chaos in Newtonian gravity. This may also be true in a relativistic system such as the evolution of a binary system. The motion of coalescing binary systems of neutron stars and/or black holes is very important to study because they are promising sources of gravitational waves, which we are planning to detect by large-scale laser interferometric gravitational observatories, such as US LIGO [14]. If we will detect the signal of gravitational waves emitted from these systems and compare it with theoretical templates, we may be able to determine a variety of astrophysical parameters of the sources such as their direction, distance, masses, spin, and so on [15]. In order to extract exact information about such sources from the observed signal we need the exact theoretical templates of the gravitational wave forms. To make such templates, it is very important to know the exact motion of sources. Hence, the equations of motion in the post-Newtonian expansion in terms of a small parameter $\epsilon\approx(v/c)^2\sim GM/r$ have been studied by many authors [16]. Those can be written schematically as

$$\frac{d^2\boldsymbol{x}}{dt^2}=\boldsymbol{a}_{\rm N}+\boldsymbol{a}_{\rm PN}^{(1)}+\boldsymbol{a}_{\rm SO}^{(3/2)}+\boldsymbol{a}_{\rm 2PN}^{(2)}+\boldsymbol{a}_{\rm SS}^{(2)}+\boldsymbol{a}_{\rm RR}^{(5/2)}+O(\boldsymbol{a}^{(3)}), \quad (1.1)$$

where the subscripts N, PN, SO, 2PN, SS, and RR denote Newtonian, post-Newtonian, spin-orbit coupling, second

*Electronic address: 696L5186@cfi.waseda.ac.jp
†Electronic address: maeda@cfi.waseda.ac.jp

post Newtonian, spin-spin coupling, and radiation reaction terms, respectively [17]; and the superscript corresponds to the order of expansion in ϵ. To make sufficient templates, we may need at least the third-order post-Newtonian contribution to obtain the S/N ratio required from the observation [18–20]. But this is still under investigation in the world.

The spin effect is also important. The spin terms in Eq. (1.1), $\boldsymbol{a}_{\rm SO}$ and $\boldsymbol{a}_{\rm SS}$, induce a precession of the orbital plane through the spin-orbit or spin-spin coupling, resulting in modulation of the gravitational wave forms [21,22]. In [22], it is also shown that the orbital plane may behave very strangely due to the spin effects. We cannot verify whether or not any chaotic behavior occurs in their system. But from the studies on spin effects in Newtonian dynamics, we know that a spin effect can make a motion chaotic. We then expect that a relativistic system such as a coalescing binary pulsar may also show the similar nonlinear phenomena. The gravitational wave form from the system with chaotic motion will be different from that from a system with a regular motion, for example, a regular precession of the orbital plane as shown in [21]. The chaos might be too strong to make a complete template of gravitational waves, or rather it might give us new information about astrophysical parameters from a time series of the observed wave forms. We will discuss this problem for a coalescing binary system with highly spinning bodies elsewhere.

Thus, we believe that a study about spin effects on the orbital evolution of a relativistic system and its gravitational wave form is very important from the viewpoint of observations as well as from academic interest. In this paper, to clarify the spin effect on the orbital motion, especially the spin-orbit interaction, we study the motion of a spinning test particle around a Schwarzschild black hole. So far, studies about a spinning test particle in relativistic spacetime have been done by many authors since the basic equations were derived by Papapetrou [23] and reformulated by Dixon [24]. Corinaldesi and Papapetrou already discussed a spinning test particle in Schwarzschild spacetime [25]. But, apart from the supplementary condition, from which they adopted a different equation for the present standard one [Eq. (2.4)], they presented the basic equations and discussed some terms with physical interpretations. They did not analyze the orbits in detail from a viewpoint of the dynamical system. Kerr or Kerr-Newman spacetime was also analyzed by several authors [26–34]. In [26–28], the effective potential of the spinning particle is given and the spin effects on the binding energy are discussed. In [32,33], the gravitational waves produced by a spinning particle falling into a Kerr black hole or moving circularly around it are discussed and the energy emission rate from those systems is calculated. But in those papers they discussed only the case of the orbit in the equatorial plane or on the symmetric axis of the black hole. Since we are interested in chaotic motion induced by spin-orbit coupling here, we have to discuss the most generic situation, i.e., the orbital motion off the equatorial plane.

This paper is organized as follows. In Sec. II we shall briefly review the basic equations, i.e., the equations of motion for a spinning test particle in relativistic spacetime, a supplementary condition, and some constants of motion. We specify the background spacetime to be a Schwarzschild black hole, then we write down those equations and introduce a sort of ''effective potential,'' which enables us to classify the particle behavior. In Sec. III, performing numerical integrations, we show that chaos occurs for a highly spinning test particle. Summary and some remarks follow in Sec. IV.

Throughout this paper we use units $c=G=1$. We define the signature of the metric as $(-,+,+,+)$.

II. BASIC EQUATIONS FOR A SPINNING TEST PARTICLE

A. Pole-dipole approximation

The equations of motion of a spinning test particle in a relativistic spacetime were first derived by Papapetrou [23] and then reformulated by Dixon [24]. Those are a set of equations:

$$\frac{dx^\mu}{d\tau}=v^\mu, \tag{2.1}$$

$$\frac{Dp^\mu}{D\tau}=-\frac{1}{2}R^\mu{}_{\nu\rho\sigma}v^\nu S^{\rho\sigma}, \tag{2.2}$$

$$\frac{DS^{\mu\nu}}{D\tau}=p^\mu v^\nu-p^\nu v^\mu, \tag{2.3}$$

where τ, v^μ, p^μ, and $S^{\mu\nu}$ are an affine parameter of the orbit, the four-velocity of the particle, the momentum, and the spin tensor, respectively. τ is chosen as the proper time of the particle in this paper, then $v^\mu v_\mu=-1$. The multipole moments of the particle higher than mass monopole and spin dipole are ignored. It is called the pole-dipole approximation.

We need a supplementary condition which gives a relation between v^μ and p^μ, because p^μ is no longer parallel to v^μ in the present case. The right-hand side (RHS) of Eq.(2.2) denotes a spin-orbit coupling through a strong gravitational field. We adopt the condition [24]

$$p_\mu S^{\mu\nu}=0. \tag{2.4}$$

This condition is related to how to choose the center of mass in an extended body, and this choice gives a consistent condition [35]. Using Eq. (2.4) we can write down the relation between v^μ and p^μ explicitly, that is,

$$v^\mu=N\left[u^\mu+\frac{1}{2\mu^2\Delta}S^{\mu\nu}u^\lambda R_{\nu\lambda\rho\sigma}S^{\rho\sigma}\right], \tag{2.5}$$

where

$$\Delta=1+\frac{1}{4\mu^2}R_{\alpha\beta\gamma\delta}S^{\alpha\beta}S^{\gamma\delta}, \tag{2.6}$$

and

$$N=\left[1-\frac{1}{4\Delta^2\mu^2}S_{\mu\nu}u_\lambda S_{\rho\sigma}R^{\nu\lambda\rho\sigma}S^{\mu\alpha}u^\beta S^{\gamma\delta}R_{\alpha\beta\gamma\delta}\right]^{-1/2}, \tag{2.7}$$

is a normalization constant fixed by $v_\nu v^\nu=-1$. $u^\nu\equiv p^\nu/\mu$ is a unit vector parallel to the momentum p^ν, where the mass of the particle μ is defined by

$$\mu^2 = -p_\nu p^\nu. \tag{2.8}$$

This system has several conserved quantities. Regardless of the symmetry of the background spacetime, it is easy to show that μ and the magnitude of spin S, defined by

$$S^2 \equiv \frac{1}{2} S_{\mu\nu} S^{\mu\nu}, \tag{2.9}$$

are constants of motion [31]. If a geometry possesses some symmetry described by a Killing vector ξ^μ associated with the symmetry, we can show that

$$C \equiv \xi^\mu p_\mu - \frac{1}{2} \xi_{\mu;\nu} S^{\mu\nu} \tag{2.10}$$

is also conserved [24].

B. Spinning particle in Schwarzschild spacetime

As for the background spacetime, we assume a Schwarzschild spacetime: i.e.,

$$ds^2 = -f(r)dt^2 + f(r)^{-1}dr^2 + r^2(d\theta^2 + \sin^2\theta d\phi^2), \tag{2.11}$$

where

$$f(r) = 1 - \frac{2M}{r}, \tag{2.12}$$

with M being the mass of the black hole. Because the spacetime is static and spherically symmetric, there are two Killing vector fields, $\xi^\mu_{(t)}$ and $\xi^\mu_{(\phi)}$. From Eq. (2.10), we find the constants of motion related with those Killing vectors as

$$E \equiv -C_{(t)} = -p_t - \frac{M}{r^2} S^{tr}, \tag{2.13}$$

$$J_z \equiv C_{(\phi)} = p_\phi - r(S^{\phi r} - rS^{\theta\phi}\cot\theta)\sin^2\theta. \tag{2.14}$$

E and J_z are interpreted as the energy of the particle and the z component of the total angular momentum, respectively. Because the spacetime is spherically symmetric, the x and y components of the total angular momentum are also conserved. Then, we have two additional constants of motion as

$$J_x = -p_\theta \sin\phi - p_\phi \cot\theta\cos\phi + r^2 S^{\theta\phi}\sin^2\theta\sin\phi + rS^{\phi r}\sin\theta\cos\theta\sin\phi + rS^{r\theta}\cos\phi, \tag{2.15}$$

$$J_y = p_\theta \cos\phi - p_\phi \cot\theta\sin\phi + r^2 S^{\theta\phi}\sin^2\theta\cos\phi + rS^{\phi r}\sin\theta\cos\theta\cos\phi - rS^{r\theta}\sin\phi. \tag{2.16}$$

Because the background is spherically symmetric, without loss of generality we can choose the z axis in the direction of total angular momentum as

$$(J_x, J_y, J_z) = (0,0,J), \tag{2.17}$$

where $J > 0$. Three constraint equations (2.14)–(2.16) with Eq. (2.17) are reduced to

$$S^{\theta\phi} = \frac{J}{r^2}\cot\theta, \tag{2.18}$$

$$S^{r\theta} = -\frac{p_\theta}{r}, \tag{2.19}$$

$$S^{\phi r} = \frac{1}{r}\left(-J + \frac{p_\phi}{\sin^2\theta}\right). \tag{2.20}$$

$S^{ti}(i = r, \theta, \phi)$ are fixed from Eq. (2.4) with Eqs. (2.18)–(2.20) as

$$S^{tr} = -\frac{1}{rp_t}\left(p_\theta^2 + \frac{p_\phi^2}{\sin^2\theta} - Jp_\phi\right), \tag{2.21}$$

$$S^{t\theta} = \frac{1}{rp_t}\left(p_r p_\theta + \frac{Jp_\phi}{r}\cot\theta\right), \tag{2.22}$$

$$S^{t\phi} = -\frac{1}{rp_t}\left(Jp_r - \frac{p_r p_\phi}{\sin^2\theta} + \frac{Jp_\theta}{r}\cot\theta\right). \tag{2.23}$$

The energy conservation equation (2.13) is now

$$E = -p_t + \frac{1}{p_t r^3}\left(p_\theta^2 + \frac{p_\phi^2}{\sin^2\theta} - Jp_\phi\right). \tag{2.24}$$

The procedure to give initial conditions for calculating the orbital evolution of the particle is as follows. First, we give constants of motion S, J, and E with which the motion of the particle is bounded to a compact region of the spacetime. We will discuss how to do it in detail in the next subsection. We set the particle on the equatorial plane $\theta = \pi/2$ with $r = r_0$ and $\phi = 0$. Next, we give the spatial components of the spin tensor $\boldsymbol{S} = (S^{\theta\phi}, S^{\phi r}, S^{r\theta})$. $S^{\theta\phi}$ vanishes at $\theta = \pi/2$ from Eq. (2.18), which means that the initial spin is perpendicular to the radial direction. The last parameter we need to choose initially is,

$$\alpha \equiv \arctan\frac{S^{r\theta}}{S^{\phi r}}, \tag{2.25}$$

which determines the direction of the spin. Note that $\alpha = 0$ and π denote the spin anti-parallel and parallel to the positive z direction, respectively. In this case the orbit of the particle is always restricted to the equatorial plane and chaos never occurs. We assume $\pi/2 \leqslant \alpha \leqslant 3\pi/2$, which corresponds to the case that the z component of spin points to the same direction as that of the total angular momentum. Otherwise, since the particle cannot get into any relativistic region, the spin-orbit interaction [RHS of Eq. (2.2)] can be neglected. Then, the motion of the particle becomes same as that of a spinless particle, which is completely integrable, and chaos never occurs.

From Eq. (2.9) with Eqs. (2.18)–(2.25), we find that

$$S^{\phi r}=-\frac{p_t S}{\sqrt{J^2\sin^2\alpha+\mu^2 r_0^2}}\cos\alpha,$$

$$S^{r\theta}=-\frac{p_t S}{\sqrt{J^2\sin^2\alpha+\mu^2 r_0^2}}\sin\alpha. \tag{2.26}$$

Inserting Eqs. (2.19) and (2.20) with these equations into Eq. (2.24) (at $\theta=\pi/2$), we get the quadratic equation for u_t. Solving it and inserting the result into Eq. (2.26), we find the initial values for p_t, $\boldsymbol{S}$. p_θ, p_ϕ, and S^{ti} are determined from Eqs. (2.19)–(2.23) and p^r is given by use of Eq. (2.8).

C. Contour of zero meridian momentum as an ''effective potential''

Since we are interested in chaotic behavior of a particle orbit, we analyze a test particle which does not escape to infinity and does not fall into a black hole. Therefore, we have to choose appropriate parameters of the particle, E, J, and S. If we have an effective potential, such a choice is easy. For example, for a spinless particle traveling around a Schwarzschild black hole with the orbital angular momentum L, whose motion is restricted to a plane (e.g., the equatorial plane $\theta=\pi/2$), the effective potential of the particle is given as

$$V^2(r;L)=\left(1-\frac{2M}{r}\right)\left(\mu^2+\frac{L^2}{r^2}\right). \tag{2.27}$$

Since the region where the particle with the energy E can move is given by $V^2(r)<E^2$, it is easy to choose the energy E such that the particle will move in a compact region.

In the case of a spinning particle, because the spin-orbit coupling (2.2) is not a potential force and an additional dynamical variable, i.e., the direction of the spin, exists, we cannot find any effective potential in the two-dimensional r-θ plane. To know the region where the particle can move, however, we do not need to find an effective potential itself. Rather, we need to know only the boundary of such a region, i.e., a curve in the r-θ plane where both p^r and p^θ vanish. From Eq. (2.19), $S^{r\theta}$ also vanishes there, which means that the spin lies in the meridian plane and there remains no freedom of the spin direction ($\alpha=0$ or π). From Eq. (2.8) with $p^r=p^\theta=0$, we can set

$$p_t=-\mu f^{1/2}\cosh X,$$

$$p_\phi=\mu r\sin\theta\sinh X, \tag{2.28}$$

where $X(r,\theta)$ is an unknown function. Inserting this into Eq. (2.9) with Eqs. (2.18)–(2.20), we find the equation for X as

$$(\mu^2r^2-S^2f)\sinh^2X-2\mu Jr\sin\theta\sinh X$$
$$+(J^2-S^2)f+\frac{2M}{r}J^2\sin^2\theta=0. \tag{2.29}$$

Finally, from Eq. (2.13), we obtain the equation for such a curve as

$$E=V_{(\pm)}(r,\theta;J,S), \tag{2.30}$$

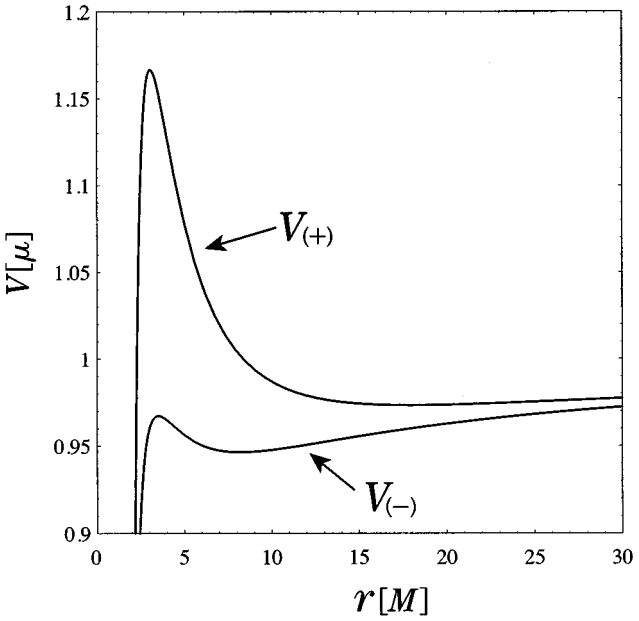

FIG. 1. The ''effective potential'' $V_{(\pm)}$ on the equatorial plane for $J=4\mu M$ and $S=1\mu M$. We see that the particle in $V_{(-)}$ moves in the region closer to the event horizon ($r=2M$) than that in $V_{(+)}$.

where

$$V_{(\pm)}(r,\theta;J,S)=\mu\left[f^{1/2}\cosh X_{(\pm)}+\frac{M\sinh X_{(\pm)}}{f^{1/2}r\cosh X_{(\pm)}}\times\left(\frac{J\sin\theta}{\mu r}-\sinh X_{(\pm)}\right)\right], \tag{2.31}$$

and

$$\sinh X_{(\pm)}\equiv\frac{\mu Jr\sin\theta}{\mu^2r^2-S^2f}\pm\left[\frac{\mu^2J^2r^2\sin^2\theta}{(\mu^2r^2-S^2f)^2}-\frac{(J^2-S^2)f+\frac{2M}{r}J^2\sin^2\theta}{\mu^2r^2-S^2f}\right]^{1/2}. \tag{2.32}$$

The subscript $(\pm)$ corresponds to the direction of the spin, i.e., if the z component of the spin is in the same direction as that of the total angular momentum ($S^{\phi r}<0$, i.e., $\pi/2<\alpha<3\pi/2$), we take $V_{(-)}$, while if it is the opposite ($S^{\phi r}>0$, i.e., $-\pi/2<\alpha<\pi/2$), $V_{(+)}$ should be applied. Note that $S^{\phi r}$ never changes its signature during the evolution. Imposing $S=0$ and $\theta=\pi/2$, $V_{(\pm)}$ is reduced to the conventional effective potential for a spinless particle in a Schwarzschild black hole, i.e., Eq. (2.27). The derivation also shows that the particle with energy E can move in the region of the r-θ plane such that $V^2_{(\pm)}(r,\theta;J,S)<E^2$. Then, we shall call $V(r,\theta;J,S)$ the ''effective potential'' of a spinning particle in Schwarzschild spacetime.

The typical shape of the potential on the equatorial plane is shown in Fig. 1. From this figure, we can see that the particle in the potential $V_{(-)}$ can move closer to the event horizon ($r=2M$) than that in the potential $V_{(+)}$. This is

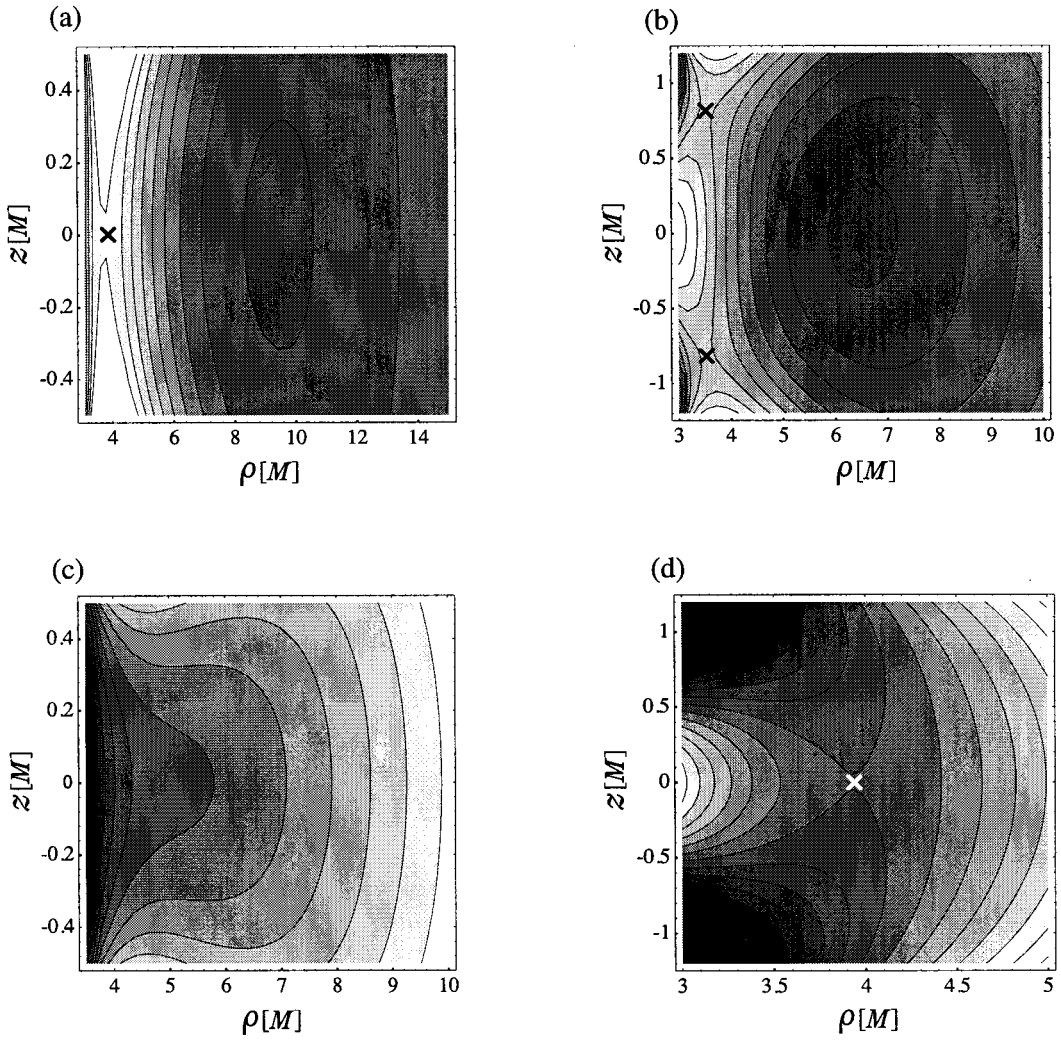

FIG. 2. Four different types of the ''effective potential'' V. The saddle point of the potential is marked by a cross. (a) Only one saddle point exists on the equatorial plane. This potential is similar to that for a spinless particle. Chaos never occurs in this case. (b) Two saddle points are found on both sides of the equatorial plane. The orbit can be chaotic. (c) When J is very small, the centrifugal force is too small to balance with the gravity and then no bound region is found. This potential is also similar to that for a spinless particle. (d) This also has no bound region. But its shape is different from that of (c). There exists a saddle point on the equatorial plane. This point is locally minimal in the r direction but maximal in θ direction. The particle will eventually fall into the black hole after leaving the equatorial plane.

because the spin-orbit interaction is a repulsive force if the spin is parallel to the orbital angular momentum and it will balance with the gravity, so that a stable periodic orbit closer to the event horizon becomes possible without falling into the black hole. If the direction of the spin is opposite, we find the reverse. Such a spin-orbit interaction is induced through the gravitational interaction as the RHS of Eq. (2.2), which breaks the integrability of the particle motion. Since we are interested in chaotic behavior, a large spin-orbit interaction may be more interesting. Hence, in this paper, we study only particle motion in a strong gravitational field, i.e., in the potential $V_{(-)}$. In what follows, we drop the subscript $(-)$.

Once J and S are given, we can depict a contour map of $V(r,\theta;J,S)$, with which we find an allowed region where a particle with E can move. We find that the ''effective potential'' V is classified into four types depending on J and S. These are given in Fig. 2. In Fig. 2(a), the potential has one saddle and one minimal point on the equatorial plane, which appears when S is small compared with J. Since the spin effect is small, the shape of the potential is similar to that for a spinless particle. We call this potential type (B1). The orbit in this case never becomes chaotic. Figure 2(b) shows the potential which has two saddle points off the equatorial plane and one minimal point on the equatorial plane. The saddle points are located symmetrically on opposite sides of the equatorial plane. We call this potential type (B2). For fixed J, as S gets larger, type (B1) changes into type (B2). This happens because a repulsive spin-orbit interaction is angle dependent. The ''effective potentials'' shown in both Figs. 2(c) and 2(d) have no bound region, although the latter case has a saddle point on the equatorial plane. The particle will eventually fall into a black hole. We call those potentials type (U1) and (U2), respectively. These potentials appear when J is small enough, i.e., the centrifugal force is too small to balance with the gravity. The type (U1) potential is similar to that for a spinless particle. In the case of type (U2), however, the situation is slightly different. Because the saddle point marked by a cross in Fig. 2(d) is minimal in the r direction and maximal in the θ direction, a particle will

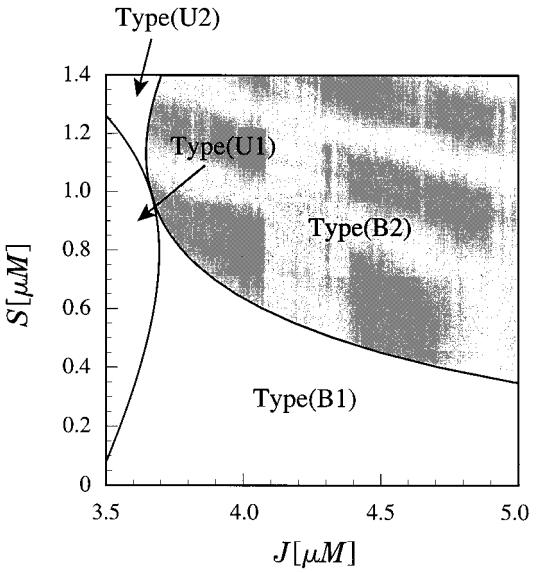

FIG. 3. The types of the ''effective potential'' are classified by J and S. The value of S at the bottom end of the type (U2) region is slightly smaller than $1\mu M$.

gradually depart from the equatorial plane and fall into a black hole. There is a potential barrier on the equatorial plane from the repulsive spin-orbit interaction.

We show in Fig. 3 what values of J and S belong to which types. Because types (B2) and (U2) never appear in the case of a spinless particle, we conclude that such strange behavior in those potentials is induced by a spin effect. As we will show later, we find that it is only for the type (B2) that the particle motion can be chaotic. Note that the value of S at the bottom end of the (U2) region is slightly smaller than $1\mu M$, i.e., at $S\sim 0.987\mu M$. Hence, the type (U2) still appears with physically meaningful values of S and J, as we will discuss soon.

III. NUMERICAL RESULTS

A. Chaos in Schwarzschild black hole

Using the Bulirsch-Stoer method [36], we integrate the equations of motion numerically for various values of parameters E, J, and S and various initial configurations of r_0 and α. As for the dynamical variables, we solve all components of the position vector x^μ, of the momentum p^μ, and of the spin tensor $S^{\mu\nu}$, and use the constraint equations (2.4),(2.8),(2.9), (2.13)–(2.16) to check the accuracy of our numerical integration. After 10^3 orbital periods, which is the end of our numerical calculation, the relative errors are smaller than 10^{-11} for each constraint. The methods with which we analyze the chaotic behavior are the Poincaré map and the Lyapunov exponent. To make the Poincaré map, we adopt the equatorial plane ($\theta=\pi/2$) as a Poincaré section and plot the point (r,v^r) when the particle crosses the Poincaré section with $v^\theta<0$. If the motion is not chaotic, the plotted points form a closed curve in the two-dimensional r-v^r plane, because a regular orbit will move on a torus in the phase space and the curve is a cross section of the torus. If the orbit is chaotic, some of those tori will be broken and the Poincaré map does not consist of a set of closed curves but the points will be distributed randomly in the allowed region. From the distribution of the points in Poincaré map, we can judge whether or not the motion is chaotic. The Lyapunov exponent is another method to judge the occurrence of chaos and it also gives a naive estimation of the strength of chaos quantitatively. This denotes how fast the close orbits in the phase space will diverge in future. The Lyapunov exponent λ is defined by

$$\lambda \equiv \lim_{t\to\infty} \frac{1}{t} \ln\left|\frac{d(t)}{d(0)}\right|, \tag{3.1}$$

where $d(t)$ is the distance at time t between two neighboring points in the phase space. If the orbit is chaotic, then λ will converge to some positive value, which means that the distance will diverge exponentially with a typical time scale $\tau_\lambda \equiv \lambda^{-1}$. For a particle moving along a geodesic, we can calculate the Lyapunov exponent by integration of the equation of geodesic deviation;

$$\frac{D^2 n^\mu}{D\tau^2} = -R^\mu{}_{\nu\rho\sigma} v^\nu n^\rho v^\sigma, \tag{3.2}$$

where n^μ is a deviation vector. In the present case, however, because a spinning test particle does not move along a geodesic as discussed in Sec. II, we need another way to estimate the Lyapunov exponent. Here, we have adopted the method developed by Sano and Sawada [37] to estimate the Lyapunov exponent. We prepare a time series of $\rho(t)$, $z(t)$, $v^\rho(t)$, and $v^z(t)$, where ρ and z are defined by $\rho \equiv r\sin\theta$ and $z \equiv r\cos\theta$, and calculate the Lyapunov exponent from such a set of data. The way to calculate the Lyapunov exponent is as follows. Let $\{\boldsymbol{x}_i | i=0,1,2,\ldots\}$ denote a set of points on some orbit in the four-dimensional phase space, i.e., $\boldsymbol{x}_i=[\rho(i\Delta t), z(i\Delta t), v^\rho(i\Delta t), v^z(i\Delta t)]$ where Δt is a small time interval. A set of ''deviation vectors'' $\{\boldsymbol{y}_i\}$ at a point $\boldsymbol{x}_i$ is defined by

$$\{\boldsymbol{y}_i\} = \{\boldsymbol{x}_{k_i} - \boldsymbol{x}_i \mid 0 < \|\boldsymbol{x}_{k_i} - \boldsymbol{x}_i\| < \epsilon\}, \tag{3.3}$$

where ϵ is a small constant chosen appropriately. After the evolution of a time interval $m\Delta t$, the orbital point $\boldsymbol{x}_i$ will proceed to $\boldsymbol{x}_{i+m}$ and neighboring points $\boldsymbol{x}_{k_i}$ to $\boldsymbol{x}_{k_i+m}$. The deviation vectors $\boldsymbol{y}_i$ are thereby mapped to

$$\boldsymbol{y}_i^{(m)} = \boldsymbol{x}_{k_i+m} - \boldsymbol{x}_{i+m}, \tag{3.4}$$

where transformation is described by a matrix $A_i^{(m)}$. Then, the Lyapunov exponent λ is calculated by

$$\lambda = \lim_{n\to\infty} \frac{1}{nm\Delta t} \sum_{i=1}^{n} \ln\|A_i^{(m)} \boldsymbol{n}^i\|, \tag{3.5}$$

where $\{\boldsymbol{n}^j\}$ is a set of arbitrary unit vectors. If the system is chaotic, λ will be positive and will not depend on choice of Δt, ϵ, m, and $\{\boldsymbol{n}^i\}$.

Figure 4 shows the Poincaré maps for the total angular momentum $J=4$ μM and for several values of the spin $S = 0.4-1.4$ μM. As for the spin of a particle with mass μ, we usually expect that $S \leqslant O(\mu^2)$. In fact, for a rotating Kerr black hole with mass M and angular momentum J, we have the inequality $J \leqslant M^2$, where the equality holds in the ex-

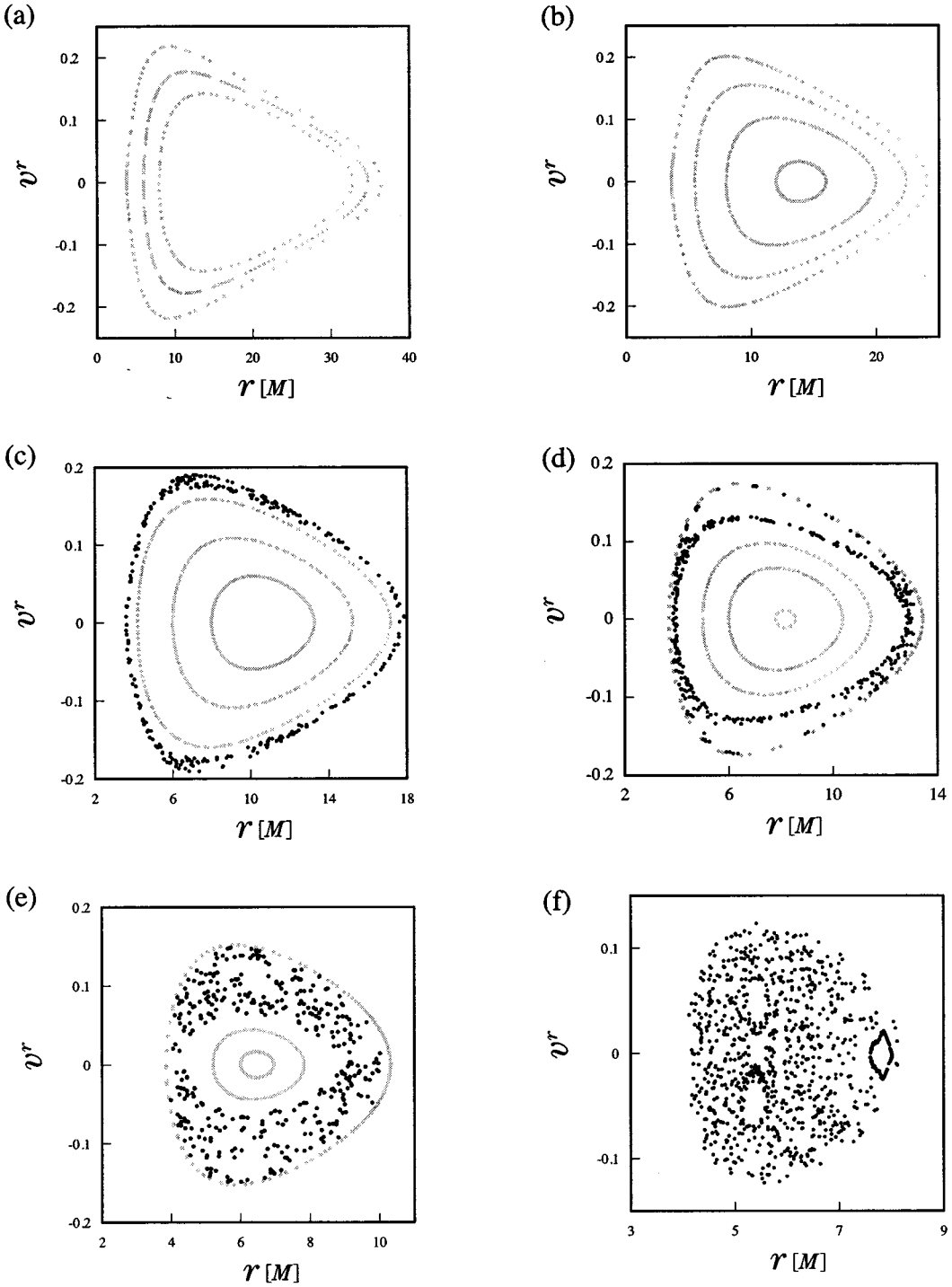

FIG. 4. The Poincaré maps for various values of S. All orbits have the total angular momentum $J=4.0\mu M$. We set $p^r=0$ initially. (a) $S=0.4\mu M$ and $E=0.976\,983\,96\mu$: The initial position for each torus is $r_0=3.8$, 6.0, and $8.0M$. (b) $S=0.6\mu M$, $E=0.967\,309\,99\mu$, and the initial position is $r_0=3.6$, 5.5, 8.0, and $12.0M$. (c) $S=0.8\mu M$, $E=0.958\,155\,68\mu$, and $r_0=3.7$, 4.2, 6.0, and $8.0M$. (d) $S=1.0\mu M$, $E=0.947\,381\,62\mu$, and (1) $r_0=5M$, (2) $3.9M$(chaotic), (3) $3.72M$. The orbits in two-dimensional configuration space are shown in Fig. 5. (e) $S=1.2\mu M$, $E=0.935\,455\,65\mu$, and $r_0=3.86$, 4.2, 5.2, and $6.0M$. (f) $S=1.4\mu M$, $E=0.922\,929\,41\mu$, and $r_0=4.5$, 5.0, 5.7, and $7.6M$. Very strong chaos occurs in this case, although it may be unrealistic.

treme limit. Therefore, for the present case, $S/\mu M=(S/\mu^2)\cdot\mu/M\leqslant O(\mu/M)$ should be much smaller than unity for a test particle, for which we assume that $\mu\ll M$. However, if we would extend our analysis to the case of a relativistic binary system with masses m_1 and m_2, we may find that $S/\mu M\sim 1$ as follows. μ and M should be regarded as the reduced and total masses, i.e., $\mu=m_1m_2/(m_1+m_2)$, $M=m_1+m_2$, and for the spin of the first relativistic star 1, $S_1/\mu M=S_1/m_1m_2=(S_1/m_1^2)\cdot m_1/m_2$. Then, we have $S_1/\mu M=S_1/m_1^2\leqslant O(1)$ for the case of $m_1=m_2$. Therefore, $S_1/\mu M$ can be large as unity. Because the value of $S=1\mu M$ is not a mathematical special bound [38], we will analyze the case of $S>1\mu M$ as well in order to see the spin effect more clearly.

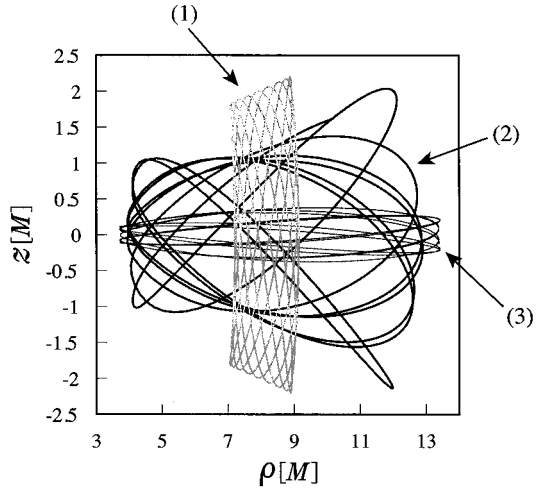

FIG. 5. The orbit in the two-dimensional configuration space corresponding to each torus in Fig. 4(d) [(1)–(3)]. (1) This orbit is almost perpendicular to the equatorial plane. The initial position is near the minimum point of the ''effective potential.'' (2) The chaotic orbit. The particle approaches the saddle points marked by a cross. (3) Contrary to the orbit shown in (1), this orbit is constrained in the very narrow area near the equatorial plane. The initial position is located near the edge of the ''effective potential.''

From Figs. 4(a) and 4(b), which correspond to the type (B1) potential, we find that the tori are not appreciably broken. Therefore, chaos is quite limited. On the other hand, in the case of the type (B2) potential, which is shown in Figs. 4(c)–4(f), we see that some tori are broken, which means that chaos occurs for such orbits. This is the first example of chaotic behavior in the motion of a test particle in a Schwarzschild spacetime. The sea of chaos spreads in these Poincaré sections as S increases. We conclude that this chaotic behavior is induced by the spin effect.

Figure 5 shows the orbit in the two-dimensional configuration space corresponding to each torus [(1)–(3)] in Fig. 4(d) ($S=1\mu M$). The orbit (1) is almost perpendicular to the equatorial plane. The initial position is near the minimum point of the ''effective potential.'' The orbit (2) is chaotic and the particle approaches the saddle points. The orbit (3) is constrained in the very narrow area near the equatorial plane contrary to the orbit (1). The initial positions are located near the edge of the ''effective potential.'' In Fig. 6, we present the Lyapunov exponents λ for orbits (1)–(3) in Fig. 5. τ_λ/T_P is also given, where T_P is the mean orbital period averaged after 10^2 rotations around a black hole. τ_λ/T_P gives a naive estimation for how many rotations we expect before the chaotic behavior becomes distinct. We may justify that the orbit (2) is strongly chaotic because of the large positive value of its Lyapunov exponent.

Is there any critical value of the spin for occurrence of chaos? If it is determined by the potential type, we obtain $S_{cr}=0.635\mu M$ for $J=4\mu M$ from Fig. 3. To confirm this, we plot the Lyapunov exponent λ in terms of the value of the spin S in Fig. 7. After S reaches the critical value S_{cr}, λ increases remarkably, which supports our conclusion.

From our numerical investigation, we find several conditions for the occurrence of chaos when setting up the initial data: A particle must move in the type (B2) potential; the particle must be bounded in a compact region, i.e.,

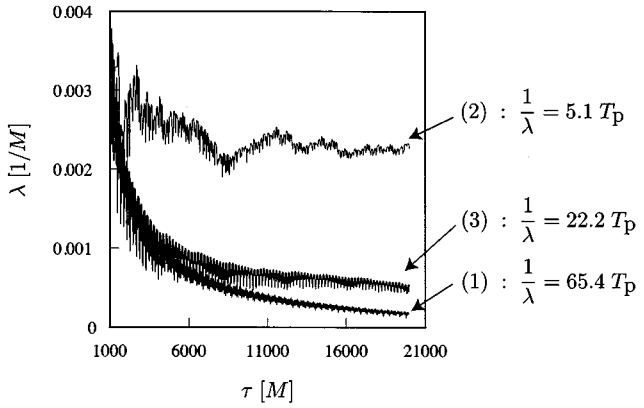

FIG. 6. The Lyapunov exponent of each orbit shown in Fig. 5. We find that the orbit (2) is strongly chaotic. The ratio of the inverse Lyapunov exponent $1/\lambda\equiv\tau_\lambda$ to the average orbital period T_P is also shown.

$E<E_{sp}$, where $E_{sp}=V(\mathbf{r}_{sp})$ is the potential energy at the saddle point $\mathbf{r}_{sp}$; the particle must have energy $E\sim E_{sp}$ and the position r_0, and the angle of the spin α must be appropriately chosen in order for the particle to approach the saddle point.

B. Transition from regular to chaos

Here, we shall briefly discuss a mechanism for the occurrence of chaos.

Figure 8 shows the Poincaré map of five orbits with $J=3.81\mu M$, $S=1\mu M$, and $E=0.923\mu$. Note that $E_{sp}=0.9288\mu$ for this case. When the value of E is small enough, the system becomes approximately integrable and we cannot see the chaotic orbit but four different types of orbits.

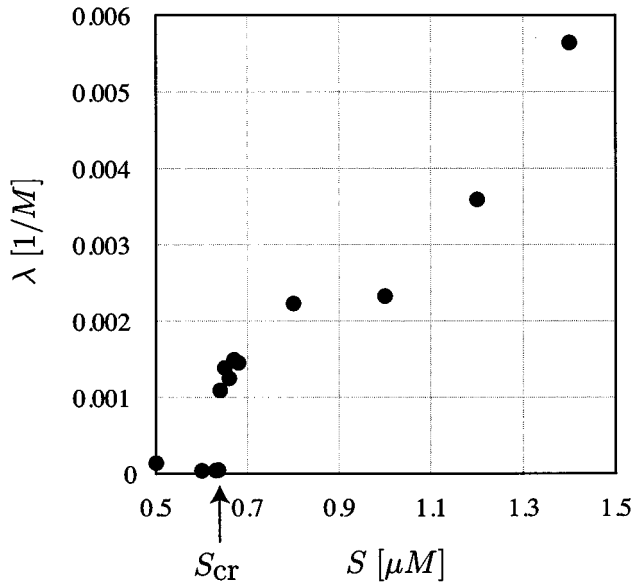

FIG. 7. The Lyapunov exponent λ in terms of the value of spin S. When S becomes larger than the critical value $S_{cr}\sim 0.635\mu M$, beyond which we find chaos, λ increases rapidly. This supports the notion of a critical value of the spin for occurrence of chaos.

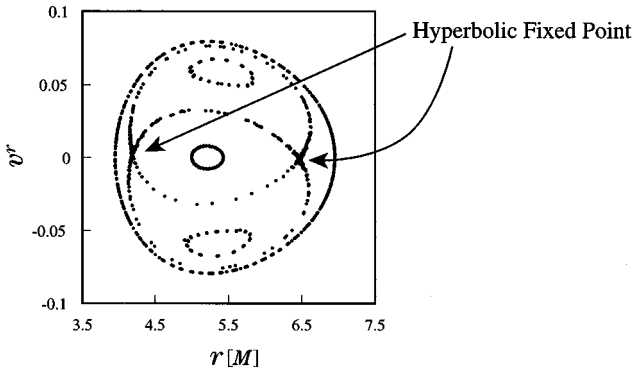

FIG. 8. The classification of the orbits for $J=3.81\mu M$, $S=1\,\mu M$, and $E=0.923\mu$. We find two separatrix [type (iv)] which divide three types of stable orbits [types (i)–(iii)]. There exists a heteroclinic orbit starting from one hyperbolic fixed point to the other fixed point, which may cause the present chaotic behaviors.

Type (i). The stable orbits which form a closed curve near the center of the Poincaré map.

Type (ii). The stable orbits which form a closed curve at the edge of the Poincaré map.

Type (iii). The stable orbits which form a closed curve in the upper or lower part of the Poincaré map.

Type (iv). The separatrix of the above three types of orbits. Two hyperbolic fixed points in this Poincaré section exist.

It is plausible that the type (iv) orbit plays an important role for the occurrence of chaos. In Fig. 8 we can see that the unstable manifold departing from one hyperbolic fixed point seems to join smoothly to the stable manifold of another hyperbolic fixed point. However, most probably, the two curves intersect at an infinity of ''heteroclinic points.'' As E increases from this state, the sea of chaos appears around the hyperbolic fixed points and spreads into whole Poincaré map. Its behavior is shown in Fig. 9. The chaos observed here may be caused by a ''heteroclinic tangle,'' although we need further detailed analysis.

The next question is what causes the existence of type (iv) orbits. Although we do not have a definite answer now, we find some correlation between an appearance of such an orbit and the type of ''effective potential.'' As S decreases, the type (ii), and then types (iii) and (iv), will vanish and only the type (i) orbit remains. This transition is seen in Fig. 4. For the case of $S=0.8\mu M$ [Fig. 4(c)], we cannot find the type (ii) orbit, and in the cases of $S=0.6$ and $0.4\mu M$ [Figs. 4(a) and 4(b)], all orbits belong to the type (i). The latter case belongs to the type (B1) potential. Hence, it seems that there exists some relation between the type of ''effective potential'' and an appearance of types (ii)–(iv) orbits. We can find some criterion for chaos using the ''effective potential.''

IV. SUMMARY AND DISCUSSION

In this paper, using the pole-dipole approximation, we study the motion of a spinning test particle near a Schwarzschild black hole to clarify its dynamical properties such as a chaos. We find that the motion of the particle can be chaotic under some appropriate conditions. Because the motion of a spinless particle in this spacetime is never chaotic because of its integrability, this chaotic behavior is purely induced by the spin-orbit interaction. The ''effective potential'' of the particle is also introduced to classify the dynamical behaviors. The ''effective potentials'' are classified into four different types depending on the total angular momentum J and the spin S. When J is large, some orbits are bounded and the ''effective potentials'' are classified into two types: for type (B1) one saddle point (unstable circular orbit) and one minimal point (stable circular orbit) on the equatorial plane exist for small spin; and for (B2) two saddle points bifurcate from the equatorial plane and one minimal point remains on the equatorial plane for large spin. If J is small, no bound orbits exist and the potentials are classified into another two types: for type (U1) no extremal point is found for small spin; and for type (U2) one saddle point appears on the equatorial plane, which is unstable in the direction perpendicular to the equatorial plane, for large spin. The types (B1) and (U1) are

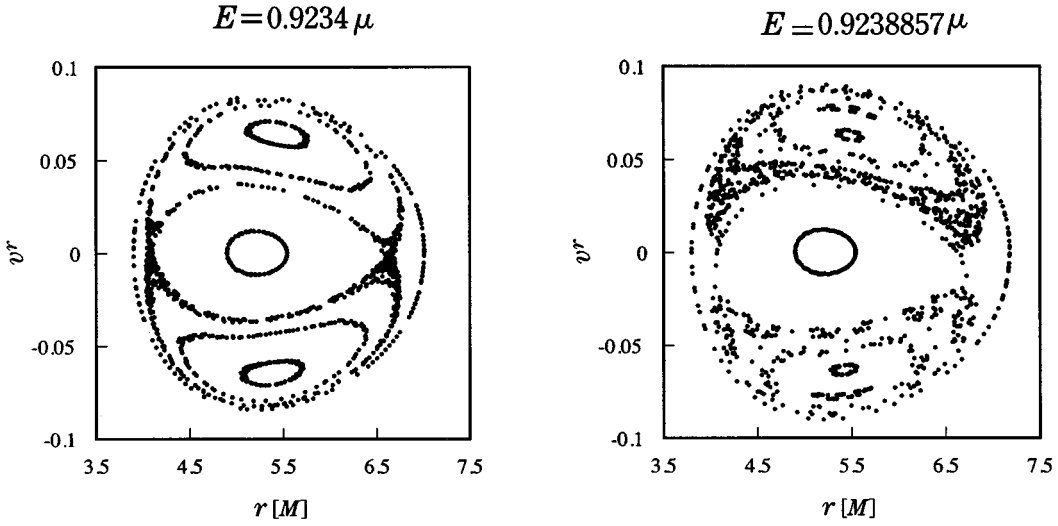

FIG. 9. When the energy increases from that in Fig. 8, the torus gradually spreads out around the heteroclinic orbit in the Poincaré map.

the same as those for a spinless particle, but the types (B2) and (U2) are new potentials which appear through a spin-orbit coupling. The chaotic behavior is found only in the type (B2) potential. We believe that the appearance of saddle points is important, because we find chaos only for the orbits which approach the saddle points.

The critical value of the spin beyond which chaos increases abruptly is $S\sim 0.635\mu M$ for $J=4\mu M$. We also present the Lyapunov exponent, which increases rapidly after the spin S gets larger than the above critical value. This supports the use of the ''effective potential'' as a criterion for chaos. The typical value of the Lyapunov exponent is about several orbital periods of the particle, which may become important in some relativistic astrophysical phenomena.

In a real astrophysical system such as a binary system, the symmetry of the system is lower than that of the present case. There may be other important effects, in addition to the spin-orbit interaction, which make the motion more complicated. Then, we may expect that chaos occurs even in the real system, or that the other effects stabilize the system and chaos will never be found. We need further analysis taking into account the other effects such as the spin-spin interaction or a force due to multipole moments, even if we adopt a test particle analysis [39]. As for the spin-spin interaction, we can analyze a spinning test particle in a rotating Kerr black hole. In our preliminary analysis by the ''effective potential'' near the equatorial plane, the critical value of the spin for chaos gets smaller as the angular momentum of the black hole becomes larger. The detailed analysis is under investigation.

Another important point is whether or not such a chaotic behavior, if it exists, affects any realistic astrophysical or physical phenomena. One of the important targets for such an investigation is a coalescing binary system, where we need general relativity, in particular relativistic dynamics of compact objects as we mentioned in Sec. I. To examine it, since we have studied here only the condition for occurrence of chaos, then we next have to know the evolution of the system including emission of gravitational waves. The particle traveling around a black hole emits the gravitational waves, extracting the energy and the angular momentum from the system. This will tell us whether or not the evolutionary path will get into the region of parameter space where chaos will take place. We then have to calculate the emission rates of the energy and the angular momentum, $\dot{E}$ and $\dot{J}$ for the present system [32,33], and follow the evolution.

ACKNOWLEDGMENTS

We would like to thank M. Sasaki, M. Shibata, Y. Sota, H. Tagoshi, and T. Tanaka for useful discussions and thank P. Haines for reading the paper carefully. S.S. also acknowledges K. Imafuku for a stimulating discussion. This work was supported partially by the Grant-in-Aid for Scientific Research Fund of the Ministry of Education, Science and Culture (Nos. 06302021 and 06640412), and by the Waseda University Grant for Special Research Projects.

APPENDIX: THE BASIC EQUATIONS BY USE OF SPIN VECTOR

In the text, we have used a spin tensor $S^{\mu\nu}$. However, it may be sometimes more convenient or more intuitive to describe the basic equations by use of a spin vector S_μ, which is defined by

$$S_\mu=-\frac{1}{2}\epsilon_{\mu\nu\rho\sigma}u^\nu S^{\rho\sigma}, \tag{A1}$$

which gives the constraint

$$p^\mu S_\mu=0. \tag{A2}$$

The equations of motion (2.1)–(2.3) are now

$$\frac{dx^\mu}{d\tau}=v^\mu, \tag{A3}$$

$$\frac{Du^\mu}{D\tau}=-\frac{1}{\mu}R^{*\mu}{}_{\nu\rho\sigma}v^\nu u^\rho S^\sigma, \tag{A4}$$

$$\frac{DS^\mu}{D\tau}=-\frac{1}{\mu}u^\mu(R^*_{\alpha\beta\gamma\delta}S^\alpha v^\beta u^\gamma S^\delta), \tag{A5}$$

where

$$R^{*\alpha\beta}{}_{\gamma\delta}\equiv\frac{1}{2}R^{\alpha\beta\rho\sigma}\epsilon_{\rho\sigma\gamma\delta}. \tag{A6}$$

The relation between the four-velocity and the momentum is

$$v^\mu=N\left(u^\mu-\frac{1}{\mu^2}{}^*R^{*\mu\alpha}{}_{\beta\gamma}S_\alpha u^\beta S^\gamma\right), \tag{A7}$$

where

$${}^*R^*_{\mu\nu\rho\sigma}\equiv\frac{1}{2}\epsilon_{\mu\nu\alpha\beta}R^{*\alpha\beta}{}_{\rho\sigma}=\frac{1}{4}\epsilon_{\mu\nu\alpha\beta}R^{\alpha\beta\gamma\delta}\epsilon_{\gamma\delta\rho\sigma}, \tag{A8}$$

and N is the normalization constant determined from $v_\mu v^\mu=-1$. The supplementary condition to fix the center of mass is

$$v_\mu S^\mu=0. \tag{A9}$$

The spin vector is perpendicular to the four-velocity as we expected. Note that $v_\mu S^{\mu\nu}\neq 0$. Equation (2.9) is just

$$S^2=S^\mu S_\mu. \tag{A10}$$

In what follow, we assume a Schwarzschild black hole as the background spacetime. We write down explicitly the relation (A1) between $S^{\mu\nu}$ and S_μ as

$$S_t=-r^2\sin\theta[u^rS^{\theta\phi}+u^\theta S^{\phi r}+u^\phi S^{r\theta}], \tag{A11}$$

$$S_r=r^2\sin\theta[u^tS^{\theta\phi}-u^\theta S^{t\phi}+u^\phi S^{t\theta}], \tag{A12}$$

$$S_\theta=r^2\sin\theta[u^tS^{\phi r}-u^\phi S^{tr}+u^rS^{t\phi}], \tag{A13}$$

$$S_\phi=r^2\sin\theta[u^tS^{r\theta}-u^rS^{t\theta}+u^\theta S^{tr}]. \tag{A14}$$

Conversely, Eqs. (A11)–(A14) with Eqs. (2.4) and (A11), give

$$S^{\theta\phi}=-\frac{u_t}{r^2\sin\theta}\widetilde{S}_r, \tag{A15}$$

$$S^{\phi r}=-\frac{u_t}{r^2\sin\theta}\widetilde{S}_\theta, \tag{A16}$$

$$S^{r\theta}=-\frac{u_t}{r^2\sin\theta}\widetilde{S}_\phi, \tag{A17}$$

where

$$\widetilde{S}_\mu\equiv S_\mu-\frac{S_t}{u_t}u_\mu. \tag{A18}$$

Using Eqs. (2.18)–(2.23), Eqs. (A11)–(A14) are now

$$\widetilde{S}_r=\frac{J}{u_t}[-(1+fu_r^2)\cos\theta], \tag{A19}$$

$$\widetilde{S}_\theta=\frac{r}{u_t}\left[J\left(\sin\theta-fu_r\frac{u_\theta}{r}\cos\theta\right)-\frac{p_\phi}{\sin\theta}\right], \tag{A20}$$

$$\widetilde{S}_\phi=\frac{r}{u_t}\left(p_\theta\sin\theta-Jfu_r\frac{u_\phi}{r}\cos\theta\right), \tag{A21}$$

$$S_t=J\left(-fu_r\cos\theta+\frac{u_\theta}{r}\sin\theta\right). \tag{A22}$$

This expression already includes the constants of motion for the angular momentum.

The initial direction of the spin vector at $r=r_0$, $\theta=\pi/2$, $\phi=0$ is given by the equations

$$\widetilde{S}_r=0, \tag{A23}$$

$$\widetilde{S}_\theta=\frac{r}{u_t}(J-p_\phi), \tag{A24}$$

$$\widetilde{S}_\phi=\frac{r}{u_t}p_\theta. \tag{A25}$$

As for the angle of the spin α, we find that

$$\alpha=\arctan\frac{\widetilde{S}_\phi}{\widetilde{S}_\theta}. \tag{A26}$$

Using this definition with (A10), we have

$$\widetilde{S}_\theta=\frac{\mu S r_0^2}{\sqrt{\mu^2 r_0^2+J^2\sin^2\alpha}}\cos\alpha, \tag{A27}$$

$$\widetilde{S}_\phi=\frac{\mu S r_0^2}{\sqrt{\mu^2 r_0^2+J^2\sin^2\alpha}}\sin\alpha. \tag{A28}$$

u_θ, u_ϕ are then some functions of u_t through Eqs. (A24) and (A25). Inserting them into the energy conservation equation (2.24), we obtain the quadratic equation for u_t. We also have Eq. (2.8) for u_r. Solving them, we can finally set up the initial data of u^μ and S^μ.

Setting $p_r=p_\theta=0$ and using Eqs. (2.8) and (A10), we find the ''effective potential'' (2.30). After giving J, S, and E and setting initial data, we can solve the dynamical equations (A3) and (A4) with algebraic equations (A7), (A19)–(A22), although here we have solved for all variables using the dynamical equations in order to estimate the accuracy by the constraint equations.

[1] J. Moser, Math. Intelligencer **1**, 65 (1978).
[2] J. Wisdom, Proc. R. Soc. London **A413**, 109 (1987).
[3] C. W. Misner, Phys. Rev. Lett. **22**, 1071 (1969).
[4] V. A. Belinskii, I. M. Khalatnikov, and E. M. Lifshitz, Adv. Phys. **19**, 525 (1970).
[5] J. D. Barrow, Phys. Rep. **85**, 1 (1982).
[6] Y. Sota, S. Suzuki, and K. Maeda, Class. Quantum Grav. **13**, 1241 (1996).
[7] G. Contopoulos, Proc. R. Soc. London **A431**, 183 (1990); **A435**, 551 (1991).
[8] C. P. Dettmann, N. E. Frankel, and N. J. Cornish, Phys. Rev. D **50**, R618 (1994).
[9] U. Yustsever, Phys. Rev. D **52**, 3176 (1995).
[10] V. Karas and D. Vokrouhlický, Gen. Relativ. Gravit. **24**, 729 (1992).
[11] H. Varvoglis and D. Papadopoulos, Astron. Astrophys. **261**, 664 (1992).
[12] L. Bombelli and E. Calzetta, Class. Quantum Grav. **9**, 2573 (1992).
[13] R. Moeckel, Commun. Math. Phys. **150**, 415 (1992).
[14] A. Abromovici, W. E. Althouse, R. W. P. Drever, Y. Gürsel, S. Kawamura, F. J. Raab, D. Shoemaker, L. Sievers, R. E. Spero, K. S. Thorne, R. E. Vogt, R. Weiss, S. E. Whitcomb, and M. E. Zucker, Science **256**, 325 (1992).
[15] C. Cutler, T. A. Apostolatos, L. Bildsten, L. S. Finn, E. E. Franagan, D. Kennefick, D. M. Markovic, A. Ori, E. Poisson, G. J. Sussman, and K. S. Thorne, Phys. Rev. Lett. **70**, 2984 (1993).
[16] For a review, see, e.g., T. Damour, in *300 Years of Gravitation*, edited by S. W. Hawking and W. Israel (Cambridge University Press, Cambridge, England, 1987), p. 128.
[17] C. M. Will, Report No. WUGRAV-94-3, gr-qc/9403033 (unpublished).
[18] C. Cutler and E. E. Franagan (work in progress).
[19] H. Tagoshi and T. Nakamura, Phys. Rev. D **49**, 4016 (1994).
[20] H. Tagoshi and M. Sasaki, Prog. Theor. Phys. **92**, 745 (1994).
[21] L. E. Kidder, Phys. Rev. D **52**, 821 (1995).
[22] T. A. Apostolatos, C. Cutler, G. J. Sussman, and K. S. Thorne, Phys. Rev. D **49**, 6274 (1994).
[23] A. Papapetrou, Proc. R. Soc. London **A209**, 248 (1951).
[24] W. G. Dixon, Proc. R. Soc. London **A314**, 499 (1970); **A319**, 509 (1970); Gen. Relativ. Gravit. **4**, 193 (1973); Philos. Trans.

R. Soc. London **277**, 59 (1974); in *Isolated Gravitating Systems in General Relativity*, edited by J. Ehlers (North-Holland, Amsterdam, 1979), p. 156.
[25] E. Corinaldesi and A. Papapetrou, Proc. R. Soc. London **A209**, 259 (1951).
[26] S. N. Rasband, Phys. Rev. Lett. **30**, 111 (1973).
[27] K. P. Tod and F. de Felice, Nuovo Cimento B **34**, 365 (1976).
[28] R. Hojman and S. Hojman, Phys. Rev. D **15**, 2724 (1977).
[29] M. A. Abramowicz and M. Calvani, Mon. Not. R. Astron. Soc. **189**, 621 (1979).
[30] E. Wald, Ann. Phys. (N.Y.) **83**, 548 (1974).
[31] E. Wald, Phys. Rev. D **6**, 406 (1972).
[32] Y. Mino, M. Shibata, and T. Tanaka, Phys. Rev. D **53**, 622 (1996).
[33] T. Tanaka, Y. Mino, M. Sasaki, and M. Shibata, Phys. Rev. D **54**, 3762 (1996).
[34] R. Rüdiger, Proc. R. Soc. London **A375**, 185 (1981); **A385,** 229 (1983).
[35] W. Beiglböck, Commun. Math. Phys. **5**, 106 (1967).
[36] W. Press, B. P. Flannery, S. Teukolsky, and W. T. Vetterling, *Numerical Recipies in C* (Cambridge University Press, Cambridge, England, 1986).
[37] M. Sano and Y. Sawada, Phys. Rev. Lett. **55**, 1082 (1985).
[38] To find a nonsingular ''effective potential,'' S should be smaller than $2\sqrt{2}\mu M$.
[39] Recently, it has been pointed out that deformation of a neutron star by a tidal force may change the innermost stable orbit in a binary system [see Lai, F. A. Raiso, and S. L. Shapiro, Astrophys. J. **420**, 811 (1994)]. It is one of the most important effects on observation of gravitational waves.